ACS OMEGA

http://pubs.acs.org/journal/acsodf

Article

Synthesis, Crystal Structures, and Density Functional Theory Studies of Two Salt Cocrystals Containing Meldrum's Acid Group

Wulan Zeng,* Xia Wang, and Yunju Zhang

Cite This: *ACS Omega* 2022, 7, 25132−25139

Read Online

ACCESS | Metrics & More | Article Recommendations

ABSTRACT: Two salt cocrystals, $C_{31}H_{34}N_4O_8$ (**DDD**) and $C_{17}H_{20}N_2O_8$ (**MDD**), were synthesized and their structures were determined by single-crystal X-ray diffraction. **DDD** is made up of one $(C_{13}H_{13}O_8)^-$ anion, one $(C_9H_{11}N_2)^+$ cation, and one 5,6-dimethyl-1*H*-benzo[*d*]imidazole molecule. **MDD** consists of one $(C_4H_7N_2)^+$ cation and one $(C_{13}H_{13}O_8)^-$ anion. **DDD** and **MDD** belong to the monoclinic, $P2_1/c$ space group and triclinic, $P\text{-}1$ space group, respectively. A 1D-chained structure of **DDD** was constituted by N−H···N and N−H···O hydrogen bonds. However, a 1D-chained structure of **MDD** was bridged by N−H···O hydrogen bonds. Their density functional theory-optimized geometric structures with a B3LYP/6-311G(d,p) basis set fit well with those of crystallographic studies. By calculating their thermodynamic properties, the correlation equations of $C^0_{p,m}$, S^0_m, H^0_m, and temperature T were obtained. By comparing the experimental electronic spectra with the calculated electronic spectra, it is found that the PBEPBE/6-311G(d,p) method can simulate the UV−Vis spectra of **DDD** and **MDD**. In addition, the fluorescence spectra in the EtOH solution analysis show that the yellowish-green emission occurs at 570 nm (λ_{ex} = 310 nm) for **DDD** and the purplish-blue emission occurs at 454 nm (λ_{ex} = 316 nm) for **MDD**.

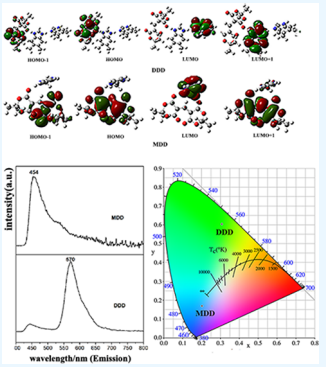

1. INTRODUCTION

As an important kind of *N*-heterocycle, imidazole and its derivatives have been widely applied in various fields including medicinal chemistry,[1] bio-organic chemistry,[2] fuel cells and solar cells,[3,4] mild steel corrosion,[5] electrocatalysts,[6] agriculture,[7] industry,[8] organic light-emitting diodes (OLEDs),[9,10] colorimetric and fluorometric chemosensors,[11] and luminescent materials.[12] As another kind of *N*-heterocycle, benzimidazole and its derivatives have also received significant attention owing to their potential applications in fluorescent sensors,[13,14] fluorescent probes,[15] chemodosimeters,[16] OLEDs,[17] and phosphorescent organic light-emitting diodes (PhOLEDs).[18]

Recently, Meldrum's acid plays an increasingly important role in the synthesis of pharmacologically active compounds such as dual inhibitors of AChE and BChE in the treatment of Alzheimer's disease,[19] antibacterial agents,[20] anticancer agents,[21] and antioxidant agents.[22] In particular, C-5-substituted derivatives of Meldrum's acid have attracted considerable interest owing to their structure and unique properties. Different synthetic routes toward the C(5)-position of Meldrum's acid have been reported.[23−26] Based on the above facts, a series of C-5-substituted derivatives of Meldrum's acid were prepared by our group during the past 10 years.[27−30] However, to the best of our knowledge, most of the reported preparation methods are step by step, and each intermediate needs to be isolated and purified. In this work, two salt cocrystals containing Meldrum's acid group are available via a simple one-pot eco-friendly method. Furthermore, less theoretical calculations or vibrational analyses have been carried out on Meldrum's derivatives coupled with a benzo[*d*]imidazole or imidazole nucleus. As a part of ongoing research, two new compounds (Chart 1), 5,6-dimethyl-1*H*-benzo[*d*]imidazol-3-ium5-((2,2-dimethyl-4,6-dioxo-1,3-dioxan-5-ylidene)methyl)-2,2-dimethyl-4,6-dioxo-1,3-dioxan-5-ide,5,6-dimethyl-1*H*-benzo[*d*]imidazole (**DDD**) and 2-methyl-1*H*-imidazol-3-ium5-((2,2-dimethyl-4,6-dioxo-1,3-dioxan-ylidene)methyl)-2,2-dimethyl-4,6-dioxo-1,3-dioxan-5-ide (**MDD**), were obtained by reacting Meldrum's acid with 5,6-dimethyl-1*H*-benzo[*d*]imidazole and 2-methyl-1*H*-imidazole in the mixture of trimethoxymethane and ethanol. Their crystal structures, vibrational frequencies, thermodynamic properties, and electronic spectra along with density functional theory (DFT) or time-dependent DFT (TD-DFT) calculational results are also reported.

Received: March 23, 2022
Accepted: June 9, 2022
Published: July 13, 2022

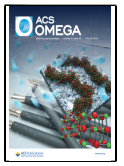

Chart 1. Synthetic Routes of MDD and DDD

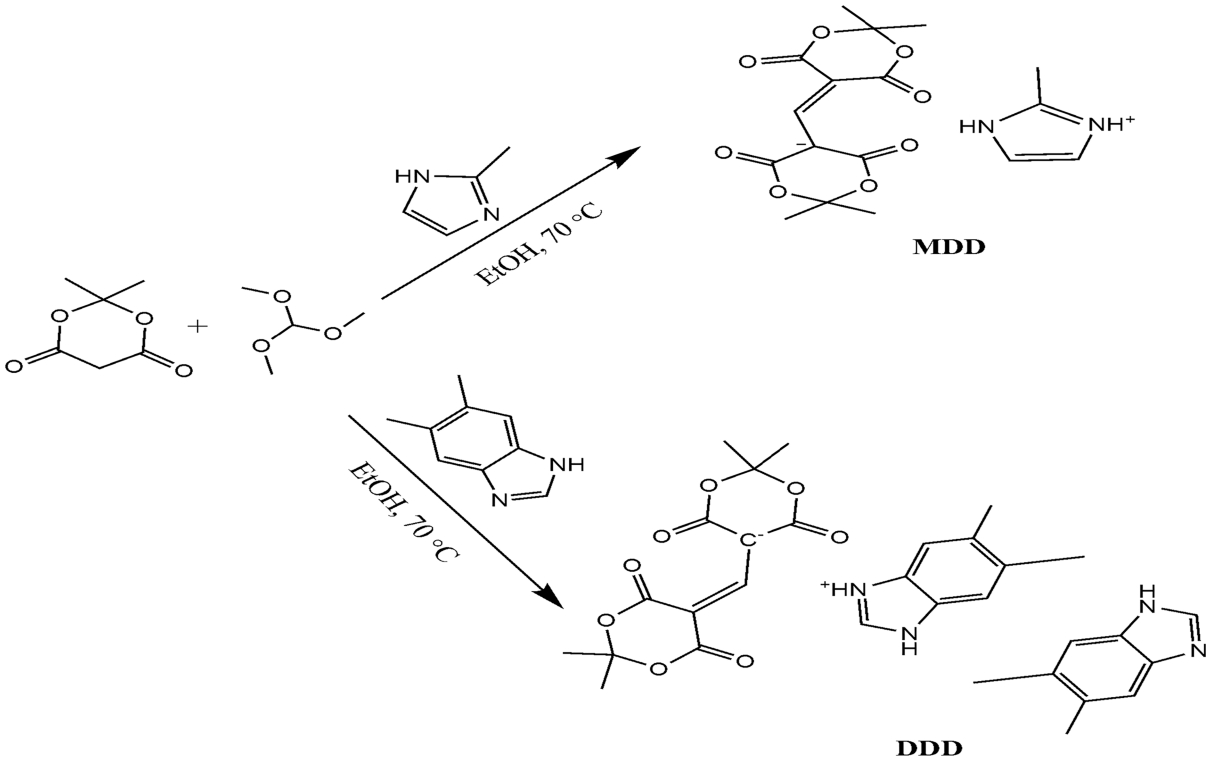

2. EXPERIMENTAL AND THEORETICAL METHODS

2.1. Physical Methods. IR data were obtained on a Nicolet 5700 FT-IR Spectrometer. The UV−Vis absorption and fluorescence spectra were collected on a TU-1901 spectrometer and an RF-5301PC fluorospectrophotometer, respectively. The C, H, and N atoms of the two compounds were recorded on an Elementar Vario EL III elemental instrument. The NMR (^{1}H and ^{13}C) spectra in $CDCl_3$ were obtained on a Bruker AVANCE III HD instrument (400 MHz).

2.2. Preparation of Two Cocrystals. The synthetic method of the two compounds was the same as that in our earlier report.[31] Briefly, a mixture of Meldrum's acid (0.72 g, 5 mmol) and trimethoxymethane (0.635 g, 6 mmol) was dissolved in EtOH (20 mL) and refluxed at 70 °C for 2−2.5 h. Then, 2-methyl-1*H*-imidazole (0.41 g, 5 mmol) was added to the reaction solution and the mixture continued refluxing for another 5 h. The solution was cooled, and the product was filtered, washed, dried, and recrystallized at room temperature in EtOH to collect red block-shaped crystals of **MDD**. Yield, 48.5%. Found: C, 53.62%; H, 5.38%; N, 7.41%. Calc. for $C_{17}H_{20}N_2O_8$: C, 53.68%; H, 5.30%; N, 7.37%. m.p.: 172.6−173.0 °C. FT-IR(KBr) cm^{-1}: 1718, 1678 (C═O), 1456 (C−N), 1275, 1190 (C−O). ^{1}H NMR (400 MHz, $CDCl_3$, δ_{ppm}): 7.52 (s, 1H), 7.00 (s, 1H), 5.45 (s, 1H), 3.53 (s, 3H), 2.73 (s, 1H), 2.18 (s, 1H), 1.76 (s, 6H), 1.25 (s, 6H). ^{13}C NMR (125 MHz, $CDCl_3$, δ_{ppm}): 150, 118, 101, 94, 26, 11.

The preparation method of **DDD** was the same as that of **MDD** except that 5,6-dimethyl-1*H*-benzo[*d*] imidazole (0.73 g, 5 mmol) replaced 2-methyl-1*H*-imidazole (0.41 g, 5 mmol) to get a red powder (**DDD**). Yield, 28.5%. m.p.: 173.8−174.5 °C. Found: C, 63.58%; H, 5.85%; N, 9.52%. Calc. for $C_{31}H_{34}N_4O_8$: C, 63.04%; H, 5.80%; N, 9.49%. FT-IR(KBr) cm^{-1}: 1698, 1633 (C═O), 1449 (C−N), 1272, 1197 (C−O). ^{1}H NMR (400 MHz, $CDCl_3$, δ_{ppm}): 14.23 (d, 1H), 9.11 (d, 1H), 8.78 (s, 1H), 7.68 (s, 3H), 5.35 (s, 1H), 3.09 (s, 6H), 2.44 (s, 6H), 2.20 (s, 3H), 1.94 (s, 6H), 1.25 (s, 6H). ^{13}C NMR (125 MHz, $CDCl_3$, δ_{ppm}): 150, 140, 134, 132, 115, 101, 94, 26, 19. Red block-shaped crystals appeared by using solvents (v petroleum ether/v acetone = 1:1).

2.3. X-ray Diffraction Analysis of DDD and MDD. The X-ray data of **DDD** and **MDD** were collected on a Spider Rapid IP (Rigaku, Japan) detector. The molecular structures of the two compounds were ascertained by SHELXL-2015 and SHELXT-2015.[32,33] The H atoms of the two compounds were placed in calculated positions and refined using the riding coordinates with C−H distances of 0.93−0.97 Å and N−H distances of 0.86 Å. $U_{iso}(H) = 1.2U_{eq}(C)$ for aromatic/amide H atoms, and $U_{iso}(H) = 1.5U_{eq}(C)$ for methyl H atoms.

2.4. Computational Methods. DFT calculations of **DDD** and **MDD** were performed with the Gaussian 09[34] package using a hybrid functional, namely, B3LYP or PBEPBE at the basis set 6-311G(d,p).[35,36] TD-DFT[37,38] calculations were used to predict the electronic spectra of the two compounds. The calculated vibrational frequencies and electronic spectra were obtained at the B3LYP/6-311G(d,p) level and the PBEPBE/6-311G(d,p) level.

3. RESULTS AND DISCUSSION

3.1. Crystal Structures of the Two Salt Cocrystals. The key parameters of the two salts are summarized in Table 1. Their molecular structures with hydrogen atoms are shown in Figure 1.

As shown in Figure 1, the molecular structure of **DDD** includes one $(C_{13}H_{13}O_8)^-$ anion, one $(C_9H_{11}N_2)^+$ cation, and one 5,6-dimethyl-1*H*-benzo[*d*]imidazole molecule. However, **MDD** consists of one $(C_{13}H_{13}O_8)^-$ and one $(C_4H_7N_2)^+$. The

https://doi.org/10.1021/acsomega.2c01761
ACS Omega 2022, 7, 25132−25139

Table 1. Crystal Structure Details for MDD and MDD[a]

	compound	
	DDD	**MDD**
formula	$C_{31}H_{34}N_4O_8$	$C_{17}H_{20}N_2O_8$
CCDC	1817941	2014484
color/shape	red/block	red/block
M_r	590.62	380.35
crystal system, space group	monoclinic, *P*21/*c*	triclinic, *P*-1
a, *b*, *c* (Å)	13.2873(6), 16.9107(6), 14.3356(6)	9.936(2), 10.556(2), 10.880(2)
α, *β*, *γ* (°)	90, 103.2430(10), 90	113.33(3) 100.27(3), 112.39(3)
crystal size (mm)	0.1 × 0.08 × 0.04	0.25 × 0.18 × 0.10
wavelength (Å)	0.71073	0.71073
θ ranges (°)	3.06−27.484	3.476−27.47
V (Å^3)	3135.5(2)	893.0(3)
Z	4	2
F(000)	1248	400
D (g·cm^{-3})	1.251	1.415
−*h*, *h*/−*k*, *k*/−*l*, *l*	−17, 17/−20, 21/−18, 18	−12, 12/−13, 13/−14, 13
total, unique, and [*I* > 2*σ*(*I*)] reflections	30,494, 7196, 2955	8248, 3960, 3295
no. of reflections, restraints, parameters	7196, 0, 396	3960, 0, 244
R(int)	0.0462	0.0393
R, *wR*, *S*	0.0541, 0.1311, 0.890	0.0539, 0.1383, 1.108
$(\Delta\rho)_{max}$, $(\Delta\rho)_{min}$ (e/Å^3)	0.290, −0.194	0.386, −0.356

[a] $w = [\sigma^2(F_o^2) + (0.0902P)^2]^{-1}$, where $P = (F_o^2 + 2F_c^2)/3$ for **DDD**; $w = [\sigma^2(F_o^2) + (0.0821P)^2 + 0.1051P]^{-1}$, where $P = (F_o^2 + 2F_c^2)/3$ for **MDD**.

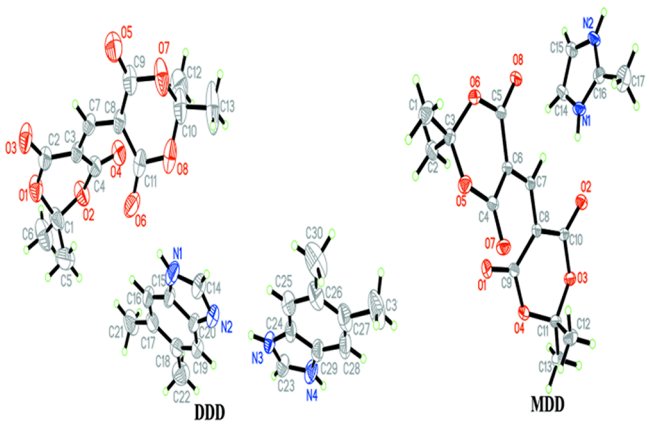

Figure 1. ORTEP drawings of **DDD** and **MDD** with 30% probability thermal ellipsoids.

central C(7) atom is bridged by two Meldrum's acid moieties, which forms the $(C_{13}H_{13}O_8)^-$ anion in the two compounds.

As shown in Table 2, bond lengths C7−C8 (1.384 (3) Å) and C7−C3 (1.374 (3) Å) (**DDD**) and C6−C7 (1.380 (2) Å) and C7−C8 (1.398 (2) Å) (**MDD**) are both larger than the C=C double bond and shorter than the C−C single bond, which form a conjugated system. Their bond angles (C3−C7=C8 (128.81 (19)°) (**DDD**) and C6−C7=C8 (130.91 (13)°) (**MDD**)) also both resemble that of our earlier report (131.19 (1)°).[31] The two 1,3-dioxane rings of the $(C_{13}H_{13}O_8)^-$ anion in the two compounds are both in a distorted envelope conformation, with their puckering parameters as follows: for ring 1 (O1, O2, C1−C4) in

Table 2. Main Bond Lengths (Å) and Bond Angles (°) by X-ray and DFT Calculations for DDD and MDD

DDD			**MDD**		
	Å			Å	
bond	exp.	calc.	bond	exp.	calc.
C7−C8	1.384(3)	1.405	C7−C8	1.398(2)	1.399
C3−C7	1.374(3)	1.385	C6−C7	1.380(2)	1.383
O5−C9	1.214(3)	1.204	O7−C4	1.2096 (19)	1.202
O6−C11	1.222(3)	1.237	O8−C5	1.2211 (17)	1.223
O8−C11	1.350(3)	1.367	O6−C5	1.3559(19)	1.361
O8−C10	1.425(4)	1.446	O6−C3	1.4450(17)	1.448
O7−C9	1.367(3)	1.391	O5−C4	1.3634(2)	1.384
O7−C10	1.432(3)	1.418	O5−C3	1.433(2)	1.422
N (1)−C (14)	1.339(3)	1.324	N1−C14	1.374(3)	1.381
N (1)−C (15)	1.377(3)	1.389	N1−C16	1.330(2)	1.332
DDD			**MDD**		
angle	(°)		angle	(°)	
C3−C7−C8	128.81(19)	132.18	C7−C8−C10	117.72(12)	117.71
C7−C8−C9	120.20(2)	116.72	C7−C8−C9	122.06(13)	123.13
C7−C8−C11	120.70(2)	124.30	C10−C8−C9	119.07(12)	118.31
C9−C8−C11	118.00(2)	118.29	C6−C7−C8	130.91(13)	132.88
C7−C3−C4	119.43(17)	116.12	C7−C6−C5	117.84(12)	116.39
C7−C3−C2	121.33(18)	124.57	C7−C6−C4	123.61(13)	123.99

DDD: *Q* = 0.4616 (2) Å, *Q* (2) = 0.4360 (2) Å, *Q* (3) = 0.1518 (2) Å, *ϑ* = 109.2 (2)°, *φ* = 243.4 (2)°; ring 2 (O7, O8, C8−C11) in **DDD**: *Q* = 0.4726 (2) Å, *Q* (2) = 0.4501 (2) Å, *Q* (3) = 0.1440 Å, *ϑ* = 72.26 (2)°, *φ* = 299.9 (2)°; ring 3 (O3, O4, C8−C11) in **MDD**: *Q* = 0.4372 Å, *Q* (2) = 0.4073 (2) Å, *Q* (3) = 0.1589 (2) Å, *ϑ* = 111.31 (3)°, *φ* = 118.5595 (2)°; ring 4 (O5, O6, C3−C6) in **MDD**: *Q* = 0.4728 (2) Å, *Q* (2) = 0.4529 (2) Å, *Q* (3) = 0.1357 (2) Å, *ϑ* = 106.68 (2)°, *φ* = 243.4468 (2)°.

In the crystal lattice of **DDD**, one kind of N−H···O intermolecular interaction and two kinds of N−H···O and N−H···N intramolecular interactions can be seen in Table 3. The two Meldrum's acid moieties of the $(C_{13}H_{13}O_8)^-$ anion are connected with the $(C_9H_{11}N_2)^+$ cation and the $C_9H_{10}N_2$ molecule by N−H···O molecular interactions, and the distances of N4···O4 and N1···O6 are 2.754 (2) and 2.743

Table 3. Intra- and Intermolecular Interactions and *π*···*π* Stacking Interactions of DDD and MDD[a]

D−H···A	symmetry	D···A (Å)	∠D−H···A (°)
MDD			
N1−H1···O2	1 − *x*, −*y*, 1 − *z*	2.723(5)	167
N2−H2···O7	1 − *x*, −*y*, −*z*	2.953 (6)	115
N2−H2···O8	−2 + *x*, *y*, −1 + *z*	2.833 (6)	157
Cg3···Cg3	−*x*, −*y*, −*z*	4.678(9)	
DDD			
N4−H4···O4	1 − *x* + 2, *y* + 1/2, −*z* + 3/2	2.754(2)	157.6
N1−H1···O6	intra	2.743(3)	171.3
N3−H3···N2	intra	2.685(2)	174.2

[a] C3 ring denotes ring N1, N2, and C14−C16.

https://doi.org/10.1021/acsomega.2c01761
ACS Omega 2022, 7, 25132−25139

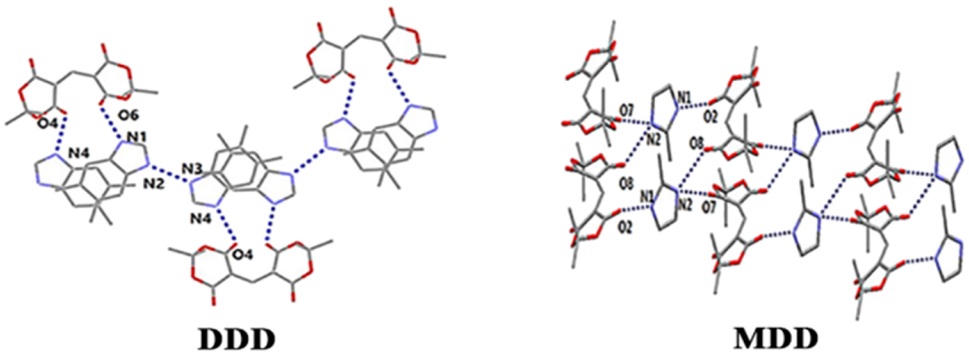

Figure 2. 1D chain of **DDD** and **MDD**.

(3) Å, respectively. However, the $(C_9H_{11}N_2)^+$ cation and $C_9H_{10}N_2$ molecule are linked by N−H···N intramolecular interactions, and the distances of N3···N2 are 2.685 (2) Å. The bond angle of N3−H3···N2 is 174.2°. The 1D-chained structure of **DDD** was connected by N−H···O intermolecular interactions (Figure 2). The 1D chain further constitutes the 3D-net structure (Figure 3).

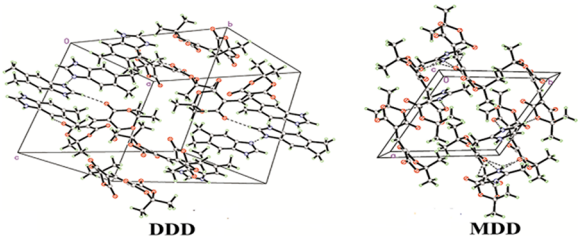

Figure 3. Packing diagrams of **DDD** and **MDD** with 30% probability thermal ellipsoids.

In the crystal lattice of **MDD**, there are three kinds of weak N−H···O intermolecular interactions and one kind of $\pi\cdots\pi$ stack interaction (Table 3). As shown in Figure 2, 2-methyl-1*H*-imidazol-3-ium links 5-((2,2-dimethyl-4,6-dioxo-1,3-dioxan-5-ylidene) methyl)-2,2-dimethyl-4,6-dioxo-1,3-dioxin-5-ide by N−H···O molecular interactions, and the distances of N (1)···O (2), N (2)···O (8), and N (2)···O (7) are 2.723 (5), 2.833 (6), and 2.953 (6) Å, respectively. The distances of $\pi\cdots\pi$ stack interactions are 4.678 (9) Å. The 1D-chained structure of **MDD** was bridged by N−H···O intermolecular interactions (Figure 2). The 3D-net network structure of **MDD** was also formed by the above 1D chain (Figure 3).

3.2. Optimization of Molecular Geometry for MDD and DDD. The optimized geometric structures of the two compounds are carried out using DFT at the B3LYP/6-311G(d,p) level, and the values are also listed in Table 2.

As shown in Table 2, most of the predicted bond lengths and angles are slightly larger than the ones measured in the experiments. It is likely because the experimental parameters of the two compounds are described in the solid state; however, the predicted values are obtained in the gas phase. Comparing the predicted values with the experimental ones, it can be found that the maximum differences in bond lengths and bond angles are 0.025 Å and 3.60° (**DDD**) and 0.011 Å and 1.97° (**MDD**), respectively, indicating that the predicted results are satisfactory and the B3LYP/6-311G(d,p) level is suitable to simulate the two crystal structures.

3.3. Thermodynamic Properties. Three main thermodynamic properties (capacity ($C^0_{p,m}$), entropy (S^0_m), and enthalpy (H^0_m)) of **MDD** and **DDD** are listed in Table 4. As shown in Table 4, all the values of thermodynamic parameters increase with the temperature rising from 100.0 to 1000.0 K,[39] which is mainly due to the enhancement of the two molecular vibrations when the temperature rises.

The correlation equations of $C^0_{p,m}$, S^0_m, H^0_m, and temperature T are as follows:

MDD:

$$C^0_{p,m} = 44.478 + 1.459T - 6.163 \times 10^{-4}T^2 \ (R^2 = 0.99975)$$

Table 4. Thermodynamic Parameters of MDD and DDD

	$C^0_{p,m}$ (J/(mol K))		H^0_m (kJ/mol)		S^0_m (J/(mol K))	
T (K)	**MDD**	**DDD**	**MDD**	**DDD**	**MDD**	**DDD**
100.0	186.78	286.25	11.08	17.16	438.20	609.60
200.0	308.42	482.93	35.97	55.80	605.89	869.59
298.1	422.22	669.05	71.84	112.34	750.32	1097.15
300.0	424.33	672.52	72.63	113.58	752.94	1101.29
400.0	532.50	852.01	120.57	189.96	890.13	1319.80
500.0	624.93	1006.90	178.59	283.14	1019.20	1527.07
600.0	700.64	1134.50	244.99	390.42	1140.06	1722.31
700.0	762.34	1238.87	318.24	509.26	1252.85	1905.29
800.0	813.14	1324.96	397.09	637.59	1358.07	2076.52
900.0	855.46	1396.75	480.58	773.77	1456.36	2236.85
1000.0	891.08	1457.19	567.96	916.55	1548.38	2387.22

https://doi.org/10.1021/acsomega.2c01761
ACS Omega 2022, 7, 25132−25139

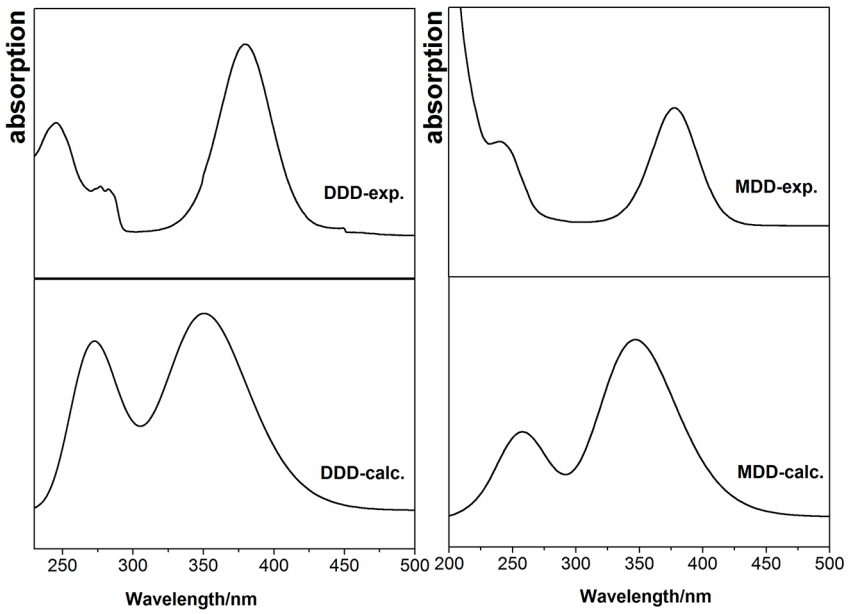

Figure 4. Experimental and calculated UV−Vis spectra of **DDD** and **MDD**.

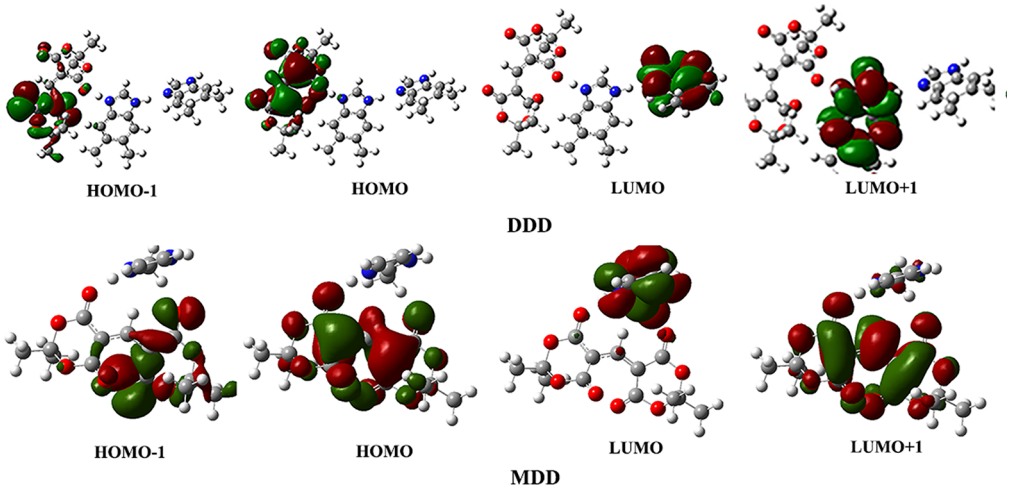

Figure 5. Charge densities of four frontier molecular orbitals for **DDD** and **MDD**.

$$S^0_m = 279.222 + 1.695T - 4.304 \times 10^{-4}T^2 \ (R^2 = 0.99989)$$

$$H^0_m = -19.263 + 0.202T + 3.904 \times 10^{-4}T^2 \ (R^2 = 0.99944)$$

DDD:

$$C^0_{p,m} = 49.99478 + 2.391T - 9.882 \times 10^{-4}T^2 \ (R^2 = 0.99972)$$

$$S^0_m = 358.254 + 2.654T - 6.289 \times 10^{-4}T^2 \ (R^2 = 0.99994)$$

$$H^0_m = -29.449 + 0.302T + 6.531 \times 10^{-4}T^2 \ (R^2 = 0.99944)$$

3.4. Electronic Analysis. The experimentally obtained absorption spectra of the two compounds in EtOH and the calculated spectra in the gas state using the TD-DFT method at the PBEPBE/6-311G(d,p) level are shown in Figure 4.

The two compounds both present two absorption bands at 245 and 379 nm (**DDD**) and at 241 and 377 nm (**MDD**): the first absorption band is owing to the $\pi \rightarrow \pi^*$ transition of the $(C_9H_{11}N_2)^+$ cation or $(C_4H_7N_2)^+$ cation and the second band is due to the $n \rightarrow \pi^*$ transition of the $(C_{13}H_{13}O_8)^-$ anion. The results resemble those of the literature reported (243 and 384).[31] The calculated spectra of the two compounds were also found to exhibit two bands at 268 and 352 nm (**DDD**) and at 265 and 342 nm (**MDD**), which illustrates that the PBEPBE/6-311G(d,p) method can simulate the experimental electronic spectra. The charge densities of four frontier molecular orbitals of the two compounds are listed in Figure 5. The HOMO-1 and HOMO electrons are mostly localized on both the 1,3-dioxane ring and C6−C7═C8 bonds of the $(C_{13}H_{13}O_8)^-$ anion in the two compounds; however, the LUMO and LUMO+1 electrons are localized on the

https://doi.org/10.1021/acsomega.2c01761
ACS Omega 2022, 7, 25132−25139

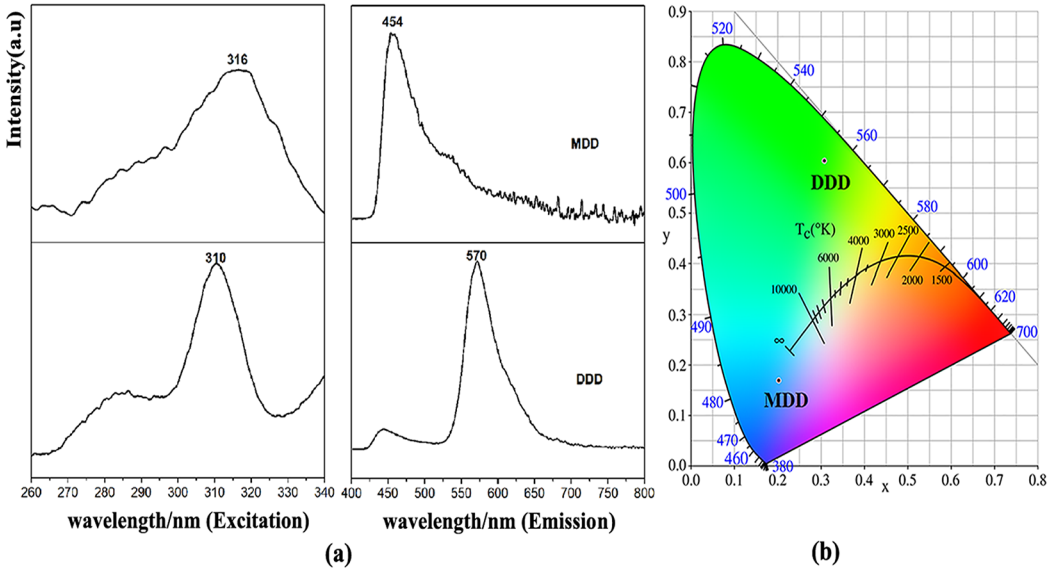

Figure 6. (a) PL spectra of **DDD** and **MDD** in EtOH solution; (b) CIE chromaticity in EtOH solution.

benzo[*d*]imidazole ring (**DDD**) and imidazole ring and C6−C7═C8 bonds (**MDD**), which are in accord with the $\pi \rightarrow \pi^*$ and $n \rightarrow \pi^*$ transitions of the experimental values. Furthermore, E_{HOMO} and E_{LUMO} of the two compounds are −0.160 and −0.086 eV for **DDD** and −0.170 and −0.076 eV for **MDD** at the PBEPBE/6-311G(d,p) levels, respectively. The energy HOMO−LUMO gap of 0.074 eV (**DDD**) is slightly smaller than that of 0.094 eV (**MDD**), which implies that the molecular structure of **MDD** is more stable.

3.5. Fluorescence Spectra. Figure 6 shows the emission and excitation spectra of the two salts and the CIE color chromaticity in EtOH solution. **DDD**'s emission band appears at 570 nm when the excitation peak is 310 nm, while the compound **MDD** shows strong emission intensity at 454 nm when the excitation peak is 316 nm. The emission band is related to the phenyl ring structure and the substituents. The emission band of **DDD** is 116 nm redshifted from the emission band of **MDD**, which is due to more phenyl rings and methyl groups. In addition, the yellowish-green region of **DDD** and the purplish-blue region of **MDD** are decided and their color coordinates (0.3075, 0.6035) and (0.2026, 0.1693) are calculated by means of CIE1931. The relation of emission spectra and the structures of **DDD** and **MDD** can provide a new idea for the design of potential fluorescent materials.

4. CONCLUSIONS

Two new salt cocrystals, $C_{31}H_{34}N_4O_8$ (**DDD**) and $C_{17}H_{20}N_2O_8$ (**MDD**), were synthesized and characterized by elemental analysis, infrared, UV−Vis, and NMR (^{1}H and ^{13}C) spectroscopy and single-crystal X-ray diffraction. Their crystal structures show that **DDD** belongs to the monoclinic, *P*21/*c* space group, and **MDD** belongs to the triclinic, *P*-1 space group. In **DDD**, the $(C_{13}H_{13}O_8)^-$ anion, $(C_9H_{11}N_2)^+$ cation, and $C_9H_{10}N_2$ molecule were linked by N−H···O and N−H···N molecular interactions. However, in **MDD**, the $(C_{13}H_{13}O_8)^-$ anion and $(C_4H_7N_2)^+$ cation were bridged by N−H···O intermolecular interactions. The optimized geometric structure using DFT at the B3LYP/6-311G(d,p) level is suitable to simulate the molecular structures of **DDD** and **MDD**. The calculated results of the two compounds with the TD-DFT method at the PBEPBE/6-311G(d,p) level are in accordance with experimental values.

■ ASSOCIATED CONTENT

Accession Codes

CCDC 1817941 (**DDD**) and 2014484 (**MDD**) contain the supplementary crystallographic data for this paper. These data can be obtained free of charge at www.ccdc.cam.ac.uk/conts/retrieving.html [or from the Cambridge Crystallographic Data Centre (CCDC), 12 Union Road, Cambridge CB2 1EZ, UK; fax: +44(0)1222-336033; email: deposit@ccdc.cam.ac.uk].

■ AUTHOR INFORMATION

Corresponding Author

Wulan Zeng − *Department of Chemistry, Chemical Engineering and Environmental Engineering, Weifang University, Weifang 261061, China;* orcid.org/0000-0001-5029-6493; Email: wulanzeng@163.com

Authors

Xia Wang − *Department of Chemistry, Chemical Engineering and Environmental Engineering, Weifang University, Weifang 261061, China*

Yunju Zhang − *School of Chemistry and Chemical Engineering, Key Laboratory of Photoinduced Functional Materials, Mianyang Normal University, Mianyang 621000, PR China*

Complete contact information is available at: https://pubs.acs.org/10.1021/acsomega.2c01761

Author Contributions

W.Z. designed the experiment, synthesized the two compounds, and wrote the draft. X.W. provided the funds. Y.Z. calculated the vibration spectra and electronic spectra. All authors have read and agreed to the published version of the manuscript.

Funding

This research was funded by the National Natural Science Foundation of China (no. 22108208) and the State Key

https://doi.org/10.1021/acsomega.2c01761
ACS Omega 2022, 7, 25132−25139

Laboratory of High-efficiency Utilization of Coal and Green Chemical Engineering (no. 2021-K02).

Notes

The authors declare no competing financial interest.

REFERENCES

(1) Almansour, A. I.; Arumugam, N.; Kumar, R. S.; Kotresha, D.; Manohar, T. S.; Venketesh, S. Design, synthesis and cholinesterase inhibitory activity of novel spiropyrrolidine tethered imidazole heterocyclic hybrids. *Bioorg. Med. Chem. Lett.* **2020**, *30*, No. 126789.
(2) Chaudhry, F.; Naureen, S.; Ashraf, M.; Al-Rashida, M.; Jahan, B.; Munawar, M. A.; Khan, M. A. Imidazole-pyrazolehybrids: synthesis, characterization and in-vitro bioevaluation against α-glucosidase enzyme with molecular docking studies. *Bioorg. Chem.* **2019**, *82*, 267−273.
(3) Yang, P.; Zhang, B.; Wu, H.; Cao, L.; He, X.; Jiang, Z. Imidazolium-functionalized carbon nanotubes crosslinked with imidazole poly(ether ether ketone) for fabricating anion exchange membranes with high hydroxide conductivity and dimension stability. *Electrochim. Acta* **2019**, *318*, 572−580.
(4) Wu, D.; Chen, W.; Wang, T.; Li, F.; Li, J.; Wang, E. Synthesis of copper(II)−imidazole complex modified sandwich-type polyoxometalates for enhancing the power conversion efficiency in dye sensitized solar cells. *Dyes Pigm.* **2019**, *168*, 151−159.
(5) Ouakki, M.; Galai, M.; Rbaa, M.; Abousalem, A. S.; Lakhrissi, B.; Rifi, E. H.; Cherkaoui, M. Quantum chemical and experimental evaluation of the inhibitory action of two imidazole derivatives on mild steel corrosion in sulphuric acid medium. *Heliyon* **2019**, *5*, No. e02759.
(6) Pan, X.; Wang, X.; Wang, X.; Liu, G.; Lin, H.; Li, Y. Four octamolybdate-based complexes based on flexible bis-imidazole-bis amide ligands with different lengths: structure, electrochemical and photocatalytic properties. *Inorg. Chim. Acta* **2019**, *495*, No. 118998.
(7) Blaskievicz, S. F.; Endo, W. G.; Zarbin, A. J. G.; Orth, E. S. Magnetic nanocatalysts derived from carbon nanotubes functionalized with imidazole: towards pesticide degradation. *Appl. Catal., B* **2020**, *264*, No. 118496.
(8) Huo, S.; Yang, S.; Wang, J.; Cheng, J.; Zhang, Q.; Hu, Y.; Ding, G.; Zhang, Q.; Song, P. A liquid phosphorus-containing imidazole derivative as flame-retardant curing agent for epoxy resin with enhanced thermal latency, mechanical, and flame-retardant performances. *J. Hazard. Mater.* **2020**, *386*, No. 121984.
(9) Tagare, J.; Dubey, D. K.; Jou, J. H.; Vaidyanathan, S. Synthesis, photophysical, theoretical and electroluminescence study of triphenylamine-imidazole based blue fluorophores for solution-processed organic light emitting diodes. *Dyes Pigm.* **2019**, *160*, 944−956.
(10) Jia, Y.; Wu, S.; Zhang, Y.; Fan, S.; Zhao, X.; Liu, H.; Dong, X.; Wang, S.; Lia, X. Achieving non-doped deep-blue OLEDs by applying bipolar imidazole derivatives. *Org. Electron.* **2019**, *69*, 289−296.
(11) Mahnashi, M. H.; Mahmoud, A. M.; Alkahtani, S. A.; Ali, R.; El-Wekil, M. M. A novel imidazole derived colorimetric and fluorometric chemosensor for bifunctional detection of copper (II) and sulphide ions in environmental water samples. *Spectrochim. Acta A.* **2020**, *228*, No. 117846.
(12) Chen, S. S.; Li, J. L.; Li, W. D.; Guo, X. Z.; Zhao, Y. Four new transition metal coordination polymers based on mixed 4-imidazole and carboxylate−sulfonate ligands: syntheses, structures, and properties. *J. Solid State Chem.* **2019**, *277*, 510−518.
(13) Singh, N.; Jang, D. O. Benzimidazole-based tripodal receptor: highly selective fluorescent chemosensor for iodide in aqueous solution. *Org. Lett.* **2007**, *9*, 1991−1994.
(14) Maji, A.; Pal, S.; Lohar, S.; Mukhopadhyay, S. K.; Chattopadhyay, P. A new turn-on benzimidazole-based greenish-yellow fluorescent sensor for Zn2+ ions at biological pH applicable in cell imaging. *New J. Chem.* **2017**, *41*, 7583−7590.
(15) Wu, Y. C.; You, J. Y.; Jiang, K.; Wu, H. Q.; Xiong, J. F.; Wang, Z. Y. Novel benzimidazole-based ratiometric fluorescent probes for acidic pH. *Dyes Pigm.* **2018**, *149*, 1−7.
(16) Roy, S. B.; Prodhan, C.; Chaudhuri, K.; Rajak, K. K. A benzimidazole-based chemodosimeter for the fluorometric detection of Zn and Cu via 1,5 proton shifts and C−N bond cleavage. *Photochem. Photobiol. Sci.* **2017**, *16*, 1103−1116.
(17) Gao, Y.; Xu, W.; Ma, H.; Obolda, A.; Yan, W.; Dong, S.; Zhang, M.; Li, F. Novel luminescent benzimidazole-substituent tris(2, 4, 6-trichlorophenyl) methyl radicals: photophysics, stability, and highly efficient red-orange electroluminescence. *Chem. Mater.* **2017**, *29*, 6733−6739.
(18) Huang, J. J.; Hung, Y. H.; Ting, P. L.; Tsai, Y. N.; Gao, H. J.; Chiu, T. L.; Lee, J. H.; Chen, C. L.; Chou, P. T.; Leung, M. K. Orthogonally substituted benzimidazole-carbazole benzene as universal hosts for phosphorescent organic light-emitting diodes. *Org. Lett.* **2016**, *18*, 672−675.
(19) Mehfooz, H.; Saeed, A.; Sharma, A.; Albericio, F.; Larik, F. A.; Jabeen, F.; Channar, P. A.; Flörke, U. Dual inhibition of AChE and BChE with the C-5 substituted derivative of meldrum's acid: synthesis, structure elucidation, and molecular docking studies. *Crystals* **2011**, *7*, 221−225.
(20) Bagul, S. D.; Rajput, J. D.; Bendre, R. S. Environmental chemistry letters synthesis of 3-carboxycoumarins at room temperature in water extract of banana peels. *Environ. Chem. Lett.* **2017**, *15*, 725−731.
(21) Kumar, S. S.; Biju, S.; Sadasivan, V. Synthesis, structure characterization and biological studies on a new aromatic hydrazone, 5-(2-(1,5-dimethyl-3-oxo-2-phenyl-2,3-dihydro-1H-pyrazol-4-yl) ydraz hono)-2,2-dimethyl-1,3-dioxane-4,6-dione, and its transition metal complexes. *J. Mol. Struct.* **2018**, *1156*, 201−209.
(22) Kumar, S.; Mukesh, K.; Harjai, K.; Singh, V. Synthesis of coumarin based Knoevenagel-Ugi adducts by a sequential one pot five-component reaction and their biological evaluation as antibacterial agents. *Tetrahedron Lett.* **2019**, *60*, 8−12.
(23) Dey, T.; Ghosh, S.; Ghosh, S.; Mukherjee, A. K. 5-Arylidene derivatives of Meldrum's acid: synthesis, structural characterization using single crystal and powder crystal X-ray diffraction, and electronic properties. *J. Mol. Struct.* **2015**, *1092*, 51−62.
(24) Kenchappa, R.; Bodke, Y. D.; Telkar, S.; Sindhe, M. A.; Giridhar, M. Synthesis, characterization, and antimicrobial activity of new benzofuran derivatives. *Russ. J. Gen. Chem.* **2016**, *86*, 2827−2836.
(25) Sandhu, H. S.; Sapra, S.; Gupta, M.; Nepali, K.; Gautam, R.; Yadav, S.; Kumar, R.; Jachak, S. M.; Chugh, M.; Gupta, M. K.; Suri, O. P.; Dhar, K. L. Synthesis and biological evaluation of arylidene analogues of Meldrum's acid as a new class of antimalarial and antioxidant agents. *Bioorg. Med. Chem.* **2010**, *18*, 5626−5633.
(26) Sun, X.; Anslyn, E. V. An auto-inductive cascade for the optical sensing of thiols in aqueous media: application in the detection of a VX nerve agent mimic. *Angew. Chem., Int. Ed.* **2017**, *56*, 9522−9526.
(27) Zeng, W.; Wang, X. Crystal structures of spiro derivatives including 6,10-dioxaspiro[4.5]decane-7,9-dione group and their spectral studies. *J. Chem. Crystallogr.* **2019**, *49*, 139−145.
(28) Zeng, W.; Wang, X.; Jiang, J. Design and crystal structures of two new compounds fused with 3, 4, 5-trimethoxybenzyl group and 6, 10-dioxaspiro group. *Crystals* **2018**, *8*, 146.
(29) Zeng, W.; Jian, F. 5-(2-Fluorobenzylidene)-2,2-dimethyl-1,3-dioxane-4,6-dione. *Acta Crystallogr., Sect. E: Struct. Rep. Online* **2009**, *65*, o2587.
(30) Zeng, W. 5,5-[(2,4-Dichlorophenyl)methylene]bis(2,2-dimethyl-1,3dioxane-4,6-dione). *Acta Crystallogr., Sect. E: Struct. Rep. Online* **2011**, *E67*, o1894.
(31) Zeng, W.; Jiang, J. Synthesis and crystal structure of a new hydrated benzimidazolium salt containing spiro structure. *Crystals* **2017**, *7*, 303.
(32) Sheldrick, G. M. Crystal structure refinement with SHELXL. *Acta Crystallogr., Sect. C: Cryst. Struct. Commun.* **2015**, *71*, 3−8.
(33) Sheldrick, G. M. SHELXT− Integrated space-group and crystal-structure determination. *Acta Crystallogr. Sect A* **2015**, *71*, 3−8.
(34) Frisch, M. J.; Trucks, G. W.; Schlegel, H. B.; Scuseria, G. E.; Robb, M. A.; Cheeseman, J. R.; Scalmani, G.; Barone, V.; Mennucci, B.; Petersson, G. A.; Nakatsuji, H.; Caricato, M.; Li, X.; Hratchian, H.

https://doi.org/10.1021/acsomega.2c01761
ACS Omega 2022, 7, 25132−25139

P.; Izmaylov, A. F.; Bloino, J.; Zheng, G.; Sonnenberg, J. L.; Hada, M.; Ehara, M.; Toyota, K.; Fukuda, R.; Hasegawa, J.; Ishida, M.; Nakajima, T.; Honda, Y.; Kitao, O.; Nakai, H.; Vreven, T.; Montgomery, J.A.; Peralta, J. E., Jr.; Ogliaro, F.; Bearpark, M.; Heyd, J. J.; Brothers, E.; Kudin, K. N.; Staroverov, V. N.; Keith, T.; Kobayashi, R.; Normand, J.; Raghavachari, K.; Rendell, A.; Burant, J. C.; Iyengar, S. S.; Tomasi, J.; Cossi, M.; Rega, N.; Millam, M.; Klene, M.; Knox, J. E.; Cross, J. B.; Bakken, V.; Adamo, C.; Jaramillo, J.; Gomperts, R.; Stratmann, R. E.; Yazyev, O.; Austin, A. J.; Cammi, R.; Pomelli, C.; Ochterski, J. W.; Martin, R. L.; Morokuma, K.; Zakrzewski, V. G.; Voth, G. A.; Salvador, P.; Dannenberg, J. J.; Dapprich, S.; Daniels, A. D.; Farkas, O.; Foresman, J. B.; Ortiz, J.; Cioslowski, V. J.; Fox, D. J. *Gaussian 03*; Gaussian, Inc.: Wallingford CT, 2013.

(35) Becke, A. D. A new mixing of Hartreee-Fock and local density-functional theories. *J. Chem. Phys.* **1993**, *98*, 1372−1377.

(36) Scalmani, G.; Frisch, M. J.; Mennucci, B.; Tomasi, J.; Cammi, R.; Barone, V. Geometries and properties of excited states in the gas phase and in solution: theory and application of a time-dependent density functional theory polarizable continuum model. *J. Chem. Phys.* **2006**, *124*, No. 094107.

(37) Petersilka, M.; Gossmann, U. J.; Gross, E. K. U. Excitation energies from time-dependent density-functional theory. *Phys. Rev. Lett.* **1996**, *76*, 1212.

(38) Bauernschmitt, R.; Ahlrichs, R. Treatment of electronic excitations within the adiabatic approximation of time dependent density functional theory. *Chem. Phys. Lett.* **1996**, *256*, 454−464.

(39) Khemalapure, S. S.; Hiremath, S. M.; Hiremath, C. S.; Kattia, V. S.; Basanagouda, M. M.; Khanal, G. P.; Karthick, T. Structural, spectroscopic and computational investigations on (4,6-dimethyl-benzofuran-3-yl)-acetic acid hydrazide. *J. Mol. Struct.* **2020**, *1220*, No. 128748.

https://doi.org/10.1021/acsomega.2c01761
ACS Omega 2022, 7, 25132−25139